Optical Spectra of a Novel Polyoxometalate Occluded within Modified MCM-41

Xiaoming Zhang,[†] Cheng Zhang,[‡] Haiquan Guo,[†] Wenlin Huang,[§] Tatyana Polenova,[§] Lynn C. Francesconi,[‡] and Daniel L. Akins*,[†]

Center for Analysis of Structures and Interfaces (CASI), Department of Chemistry, The City College of The City University of New York (CUNY), New York, New York 10031, Department of Chemistry, Hunter College of CUNY, New York, New York 10021, and Department of Chemistry and Biochemistry, University of Delaware, Newark, Delaware 19716

Received: May 30, 2005; In Final Form: August 20, 2005

The novel polyoxometalate ($[(Eu_2PW_{10}O_{38})_4(W_3O_8(H_2O)_2(OH)_4)]^{22-}$), also referred to herein as $Eu_8P_4W_{43}$, has been immobilized inside the channels of MCM-41 mesoporous molecular sieve material by means of the incipient wetness method. For proper host−guest interaction, amine groups were introduced into the system as a result of an aminosilylation procedure. A stable and integrated $Eu_8P_4W_{43}$ polyoxometalate was shown to be formed inside the channels of the modified MCM-41. The products were characterized by XRD, UV−vis absorption, emission, Raman excitation, Raman, and ^{31}P solid-state NMR measurements. Infrared and Raman spectra of the polyoxometalate/MCM-41 composite systems are interpreted as showing spectral shifts due to site induced electrostatic interactions. The photoluminescent behavior of the composite at room temperature indicates a characteristic Eu^{3+} emission pattern corresponding to $^5D_0-^7F_J$ transitions. A strong photoluminescence suggests the potential utility of the polyoxometalate as a luminescent material.

I. Introduction

Polyoxometalates (POMs), a class of mixed molecular, inorganic metal oxide clusters with intriguing structures and diverse properties, are a focus of contemporary materials chemistry research.[1,2] One reason for this interest has been the realization that these materials, when combined with lanthanide ions, can exhibit cooperative properties including: (i) catalytic activity for oxidation and acid-dependent reactions,[3] (ii) medicinal chemistry applications,[4] (iii) magnetism,[5,6] and (iv) useful optical properties, such as photochromism, electrochromism, and luminescence.[7−9] Thus, polyoxometalates appear to be extremely versatile building blocks for the construction of functional molecular materials.

Owing to their very low surface area and high solubility in polar solvent, it has proven necessary to incorporate POMs into stable, rigid supports, such as polymer or silica matrices and active carbon.[10,11] Among the solid matrices, mesoporous materials are promising in applications requiring large pores because of their well-defined mesoporous structures and high surface areas. Because the pores are interconnected and open, the nanoparticles within the pores are in contact with the ambient environment. Molecules can diffuse inside the pore structure of the materials, thereby, for example, making catalytically active sites available for reaction.[12]

Indeed, for a similar reason, mesoporous materials loaded with a range of nanoparticles have recently received considerable attention, especially in regards to formation of active, stable nanocatalysts.[13−16]

It is to be noted that unmodified silicate mesoporous materials contain many silanol groups, which, due to high-energy vibration of these groups, may quench the luminescence of rare earth ions. To fully exploit POM materials, such quenching interactions must be minimized. Moreover, to promote the occlusion of a POM, it is necessary to modify the interior structure of the mesoporous aluminosilicate through use of an alkoxysilane silylation reagent. This latter step can be used to promote, through appropriate functional groups, incorporation of POMs within the channels of the mesoporous molecular sieve.

In the present study, we have utilized a silylation reagent that contains an amine group, resulting in a strong interaction between the encapsulated POM and the mesoporous material (specifically, MCM-41). We specifically report on the encapsulation of $[(Eu_2PW_{10}O_{38})_4(W_3O_8(H_2O)_2(OH)_4)]^{22-}$ hereinafter referred to as $Eu_8P_4W_{43}$, within modified MCM-41. The synthesized composite material is stable and shows high luminescence, suggesting use of such nanocomposites as active agents in photoluminescent devices in environments where the luminescence of the nonencapsulated POM material would experience enhanced nonradiative relaxation. We have not made specific comparisons between our new luminescent material and others that may presently be in use in applied systems, though future efforts in our laboratories are planned that would shed light on this topic.

II. Experimental Section

Synthesis of MCM-41 and the Polyoxometalates ($Eu_8P_4W_{43}$). The POM material ($Eu_8P_4W_{43}$), polyoxotungstoeuropate, more specifically, $K_{22}[(Eu_2PW_{10}O_{38})_4(W_3O_8(H_2O)_2(OH)_4)]$, was prepared according to a method reported in the literature.[18] Figure 1 provides the X-ray crystallographically determined structure of $Eu_8P_4W_{43}$. The minor and major dimensions of this structure are ca. 20 and 25 Å, respectively.[18]

Polycrystalline aluminosilicate MCM-41 powders were prepared by using $C_{16}H_{31}(CH_3)_3NBr$ (cetyltrimethylammonium bromide, CTMABr) as the surfactant, according to refer-

* To whom correspondence should be addressed. E-mail: akins@sci.ccny.cuny.edu.
[†] The City College of The City University of New York.
[‡] Hunter College of CUNY.
[§] University of Delaware.

10.1021/jp052858m CCC: $30.25
Published on Web 09/28/2005

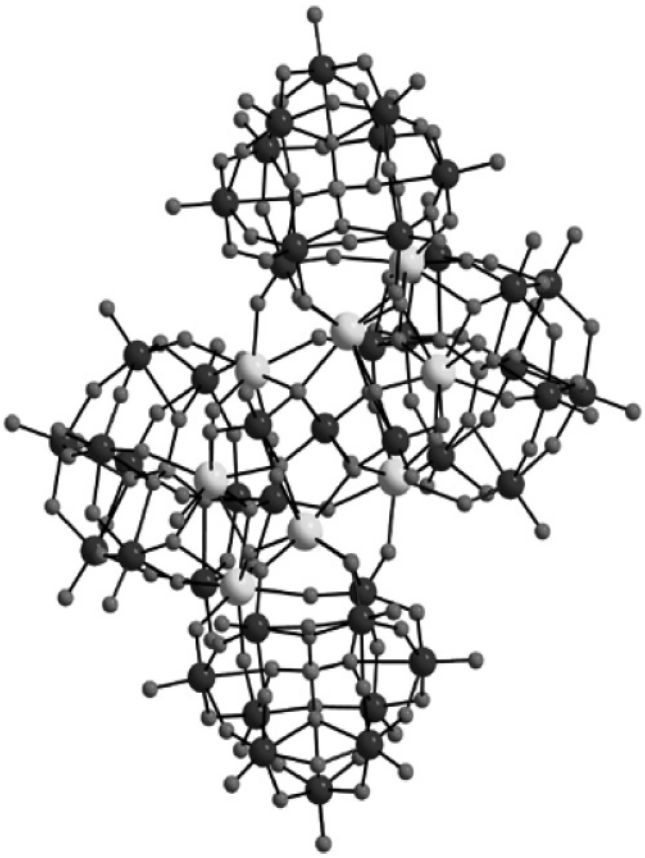

Figure 1. Ball and stick structure of the $Eu_8P_4W_{43}$ polyoxometalate. The white balls represent Eu atoms, the black balls tungsten atoms, and the gray balls phosphorus and oxygen atoms, with phosphorus lying in the centers of cages and oxygen on the peripheries.

ences.[17,19] To stabilize the synthesized MCM-41 and allow $Eu_8P_4W_{43}$ incorporation, it was necessary to modify the interior structure of MCM-41 through use of a silylation reagent (specifically, (aminopropyl)triethoxysilane, i.e., $NH_2-(CH_2)_3-Si-(C_2H_5O)_3$ (referred to as APTES)), thus linking oxygen atoms on the aluminosilicate surface, rigidifying the mesoporous framework, as well as satisfying guest−host intermolecular and/or electrostatic interactions. For our studies, the modified MCM-41 was prepared according to the method in ref 20. Briefly, about 1.5 g of the calcined MCM-41 was mixed with a chloroform solution of APTES (100 mL, 0.2 M) and stirred overnight at room temperature. The precipitate was filtered and washed with chloroform and dichloromethane.

Formation of the $Eu_8P_4W_{43}$/MCM-41 Composite. A typical ion-exchange preparation of the $Eu_8P_4W_{43}$/MCM-41 composite involved stirring a mixture of 100 mg of modified MCM-41, 100 mg of $Eu_8P_4W_{43}$, and 20 mL of distilled water for over 24 h at room temperature with the pH held at about ca. 6 using 2 M H_2SO_4. The suspension was then centrifuged, and the supernatant aqueous solution was decanted. The white powder (hereinafter designated $Eu_8P_4W_{43}$/MCM-41) was washed several times with pH 6 water to remove $Eu_8P_4W_{43}$ from the external surface and then dried in air.

Instrumentation. Steady-state emission and excitation spectra were acquired using a SPEX Fluorolog-τ2 spectrofluorometer. AFM was performed in air under ambient conditions using a ThermoMicroscopes Explorer AFM from Veeco-Digital Instruments, operated in the contact mode. The X-ray diffraction (XRD) instrument used was a Rigaku diffractometer, using Cu Kα1 (0.154 nm) X-rays, typically run at a voltage of 40 kV and current of 30 mA. IR spectra were taken on a Thermo Nicolet Auntar 360 FTIR. Raman spectra were acquired using a J-Y LabRam HR800 micro-Raman instrument, with 632.8 nm excitation provided by a HeNe laser. Nitrogen isotherms were measured using an ASAP 2010 instrument (Micromeritics) at 77 K; prior to every experiment samples were heated to 393 K and outgassed (at this temperature) under a vacuum of 10^{-5} torr. Nitrogen isotherm measurements were then used to calculate specific surface area, micropore volume, and pore size distribution. ^{31}P solid-state NMR spectra were acquired at 162.028 MHz (9.4 T) with a Tecmag Discovery spectrometer using a 4 mm Varian T3 probe; the magic angle was adjusted using $NaNO_3$ (by detecting the ^{23}Na MAS signal); a single 3 μs pulse ($\gamma H_1/2\pi = 83.3$ kHz) was employed; and a pulse delay of 1 s was used.

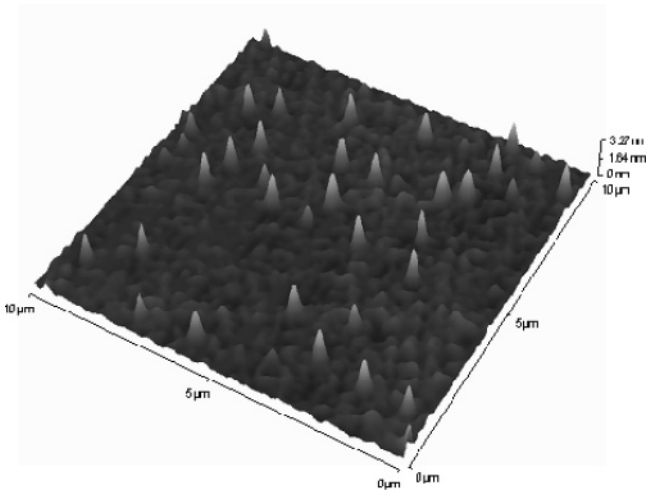

Figure 2. AFM image of the $Eu_8P_4W_{43}$ polyoxometalate spin-coated on mica.

III. Results and Discussion

Figure 2 shows the AFM image of $Eu_8P_4W_{43}$ nanoparticles spin-coated onto a mica slide. The particle's lateral size found is in the range of 1.8 to 2.7 nm, and the average height is 2.3 nm. These findings are consistent with the crystal structure estimates. Thus, the AFM topographical image suggests the presence of individual nanoparticles, which would be ideal for their incorporation into the pores of MCM-41.

The structure and pore size of MCM-41 can be evaluated by XRD and nitrogen desorption isotherm experiments. XRD patterns of pristine modified MCM-41 and the polyoxometalate-incorporated composite ($Eu_8P_4W_{43}$/MCM-41) are shown in Figure 3. With the use of Bragg's equation and comparison with reference studies, the pore size of modified MCM-41 is estimated to be ca. 27 Å. This pore size is sufficiently large to allow $Eu_8P_4W_{43}$, of approximate dimensions of 20×25 Å^2, to be incorporated. The XRD patterns of the two samples show strong (100) peaks and proportional (110) and (200) peaks, suggesting that the incorporation of the polyoxometalate into the channels does not affect the framework integrity of modified MCM-41.

For porous materials, the pore size distribution, which is based on the Kelvin equation, is a useful method for the characterization of pore structure. Figure 4 shows the nitrogen adsorption−desorption isotherms obtained at 77 K of surface-modified MCM-41 and $Eu_8P_4W_{43}$-embedded MCM-41 nanocomposite. All of the isotherms are of type IV classification, which is typical of adsorption by mesoporous materials.[21] The BET surface area, pore volume, and BJH pore diameter of the samples are listed

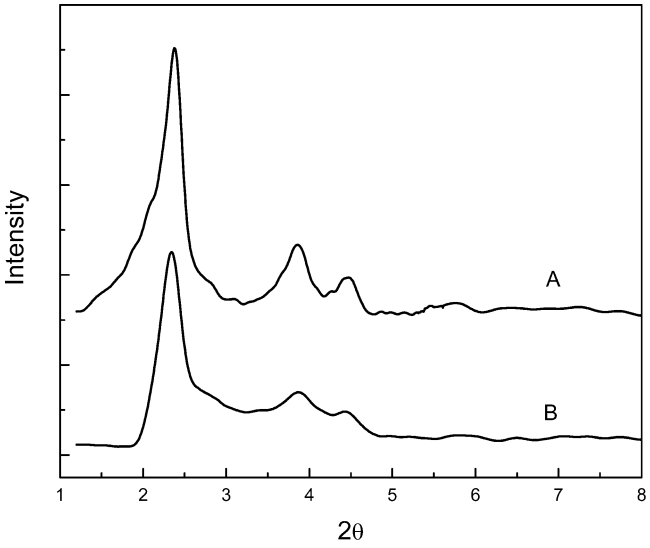

Figure 3. XRD patterns of (A) modified MCM-41 and (B) $Eu_8P_4W_{43}$/MCM-41.

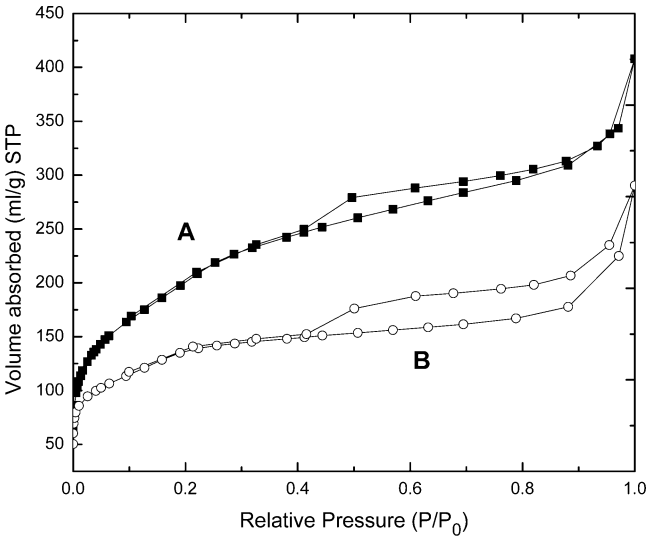

Figure 4. N_2 adsorption−desorption isotherms of (A) modified MCM-41 and (B) $Eu_8P_4W_{43}$/MCM-41.

TABLE 1: Pore Structure Parameters for Modified MCM-41 and $Eu_8P_4W_{43}$/MCM-41

samples	S_{BET} ($m^2\ g^{-1}$)	V_p ($cm^3\ g^{-1}$)	d_{BJH} (nm)
MCM-41	383.45	0.83	2.6
$Eu_8P_4W_{43}$/MCM-41	214.76	0.48	1.0

in Table 1. It is noted that introduction of polyoxometalate anions into MCM-41 leads to a decrease in surface area and pore volume. Such decrease in BET surface area, pore volume, and BJH pore diameter for $Eu_8P_4W_{43}$/MCM-41 compared to that of MCM-41 implies that $Eu_8P_4W_{43}$ nanoparticles are confined within the channels of MCM-41.[22]

Solid-state ^{31}P NMR spectra for the free $Eu_8P_4W_{43}$ and the $Eu_8P_4W_{43}$/MCM-41 nanocomposite provide further evidence that the POM structure is preserved upon incorporation into MCM-41 (Figure 5). The relative spinning sideband intensities are intact with respect to the free compound, indicating that the $Eu_8P_4W_{43}$ integrity is maintained. The broadened lines suggest that the $Eu_8P_4W_{43}$ in the nanocomposite is heterogeneous and not crystalline. In contrast, the free $Eu_8P_4W_{43}$ exhibits sharp spinning sidebands indicating a high degree

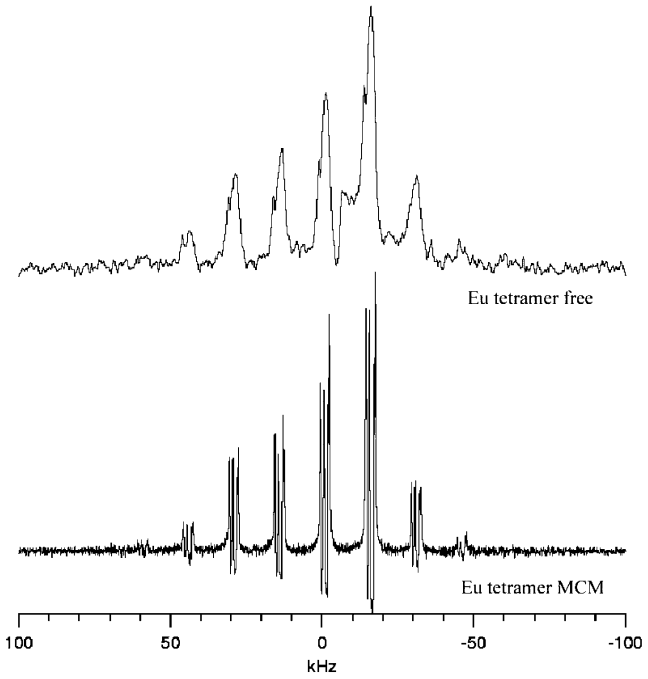

Figure 5. Solid-state ^{31}P NMR data for free $Eu_8P_4W_{43}$ (bottom) and the $Eu_8P_4W_{43}$/MCM-41 composite (top).

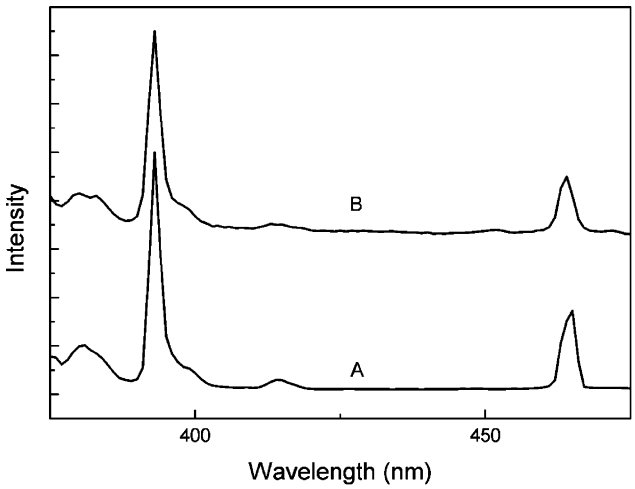

Figure 6. Excitation spectra of (A) solid $Eu_8P_4W_{43}$ and (B) composite $Eu_8P_4W_{43}$/MCM-41. Spectra were taken at 615 nm.

of crystallinity. These results suggest that the Eu tetramer has been successfully encapsulated inside the channels of MCM-41. Possible decomposition products, $(EuPW_{11}O_{39})^{4-}$ or $Eu(PW_{11}O_{39})_2$,[13] show very different sideband patterns.

The $Eu_8P_4W_{43}$ nanoparticles stabilized in MCM-41 matrices provide a unique system for studying the luminescence and photophysical properties of POM nanoparticles, since the rigid and nonconnected one-dimensional channel structure protects the particles against aggregation or precipitation in solution. The excitation spectra (Figure 6; detection wavelength of 615 nm) of both solid-state $Eu_8P_4W_{43}$ and the composite $Eu_8P_4W_{43}$/MCM-41 exhibit maximum intensities at ca. 394 nm, with the intrinsic absorption band for the composite $Eu_8P_4W_{43}$/MCM-41 being somewhat broader. All narrow peaks in the spectra are due to f−f transitions within the $4f^6$ configuration of the Eu^{3+} ion: 394 nm ($^7F_0-^5L_6$), 413 nm ($^7F_0-^5D_3$), and 466 nm ($^7F_0-^5D_2$).[23] The broad band ranging from ca. 350 to ca. 370

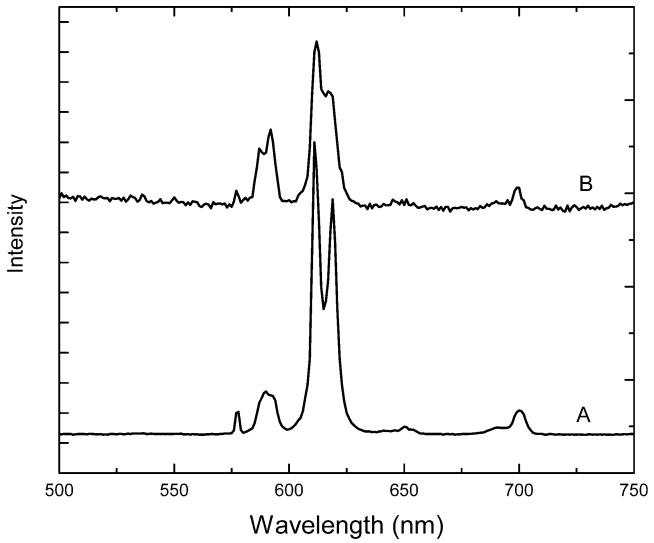

Figure 7. Emission spectra of (A) solid $Eu_8P_4W_{43}$ and (B) composite $Eu_8P_4W_{43}$/MCM-41, excited at 394 nm.

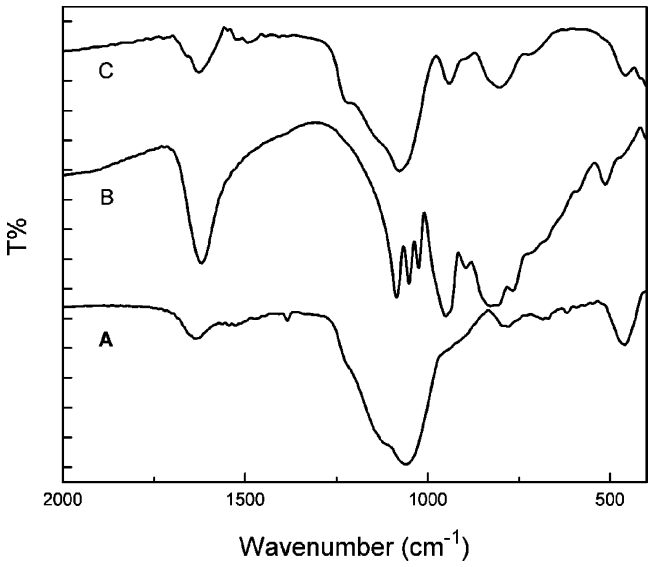

Figure 8. FTIR spectra of (A) MCM-41, (B) solid $Eu_8P_4W_{43}$ (Eu-tetramer), and (C) composite $Eu_8P_4W_{43}$/MCM-41.

nm is attributed to O−W ligand-to-metal charge transfer (LMCT).[9] It is to be noted that the excitation spectra for both samples are quite similar, indicating that the structure of the $Eu_8P_4W_{43}$ anion is not significantly altered after it enters the channels of the MCM-41, suggesting that only weak electrostatic interaction exists between the encapsulated polyoxometalate and the surface walls of MCM-41.

Emission spectra of the pure solid-state $Eu_8P_4W_{43}$ and the composite $Eu_8P_4W_{43}$/MCM-41 are shown in Figure 7. Both emission spectra exhibit bands near 536 nm (weak and not apparent in part A due to scale used) attributable to the $^5D_1 \rightarrow {}^7F_J$ transition; bands near 592 nm attributable to the $^5D_0 \rightarrow {}^7F_1$ transition; bands near 612 and 618 nm attributable to the $^5D_0 \rightarrow {}^7F_2$ transition; a band near 647 nm attributable to the $^5D_0 \rightarrow {}^7F_3$ transition; and a band near 699 nm corresponding to the $^5D_0 \rightarrow {}^7F_4$ transition.[23,24] It is to be noted that the forbidden transition $^5D_0 \rightarrow {}^7F_0$ (Eu^{3+}), which would appear at ca. 578 nm, is present in the spectra of both samples. It is well-known that the $^5D_0 \rightarrow {}^7F_0$ transition is strictly forbidden in a symmetric field. Hence, the presence of the band near 578 nm suggests that Eu^{3+} in $Eu_8P_4W_{43}$ for the two samples occupies sites with low symmetry without an inversion center.[25]

It is to be noted that the $^5D_0 \rightarrow {}^7F_1$ transition is a magnetic dipole transition, and its intensity varies with the crystal field strength acting on Eu^{3+}. On the other hand, the $^5D_0 \rightarrow {}^7F_2$ transition is an electric dipole transition and is extremely sensitive to chemical bonds in the vicinity of Eu^{3+}. Furthermore, the intensity of the $^5D_0 \rightarrow {}^7F_2$ transition increases as the site symmetry of Eu^{3+} decreases. Therefore, the intensity ratio of the $^5D_0 \rightarrow {}^7F_2$ transition compared to that of the $^5D_0 \rightarrow {}^7F_1$ transition has been widely used as a measure of the coordination state and the site symmetry of the rare earth. For the $Eu_8P_4W_{43}$ nanocomposite, the strongest emission is in the $^5D_0 \rightarrow {}^7F_2$ transition region, and the $^5D_0 \rightarrow {}^7F_2$ peak was split into two bands at 612 and 618 nm. The $^5D_0 \rightarrow {}^7F_1$ transition has the next highest intensity, and the emission peak is also split into two bands at 588 and 596 nm. The intensity ratio $I(^5D_0 \rightarrow {}^7F_2)/I(^5D_0 \rightarrow {}^7F_1)$ is found to be ca. 3.2, consistent with a low site symmetry for the Eu^{3+} ion in nanocomposite.[26]

Although excitation and emission spectra support the interpretation that $Eu_8P_4W_{43}$ is incorporated into the mesoporous MCM-41 silicate, convincing evidence for this can be ascertained by FTIR spectra. Figure 8 shows FTIR spectra of APTES-modified MCM-41, part A, and of $Eu_8P_4W_{43}$ before, part B, and after encapsulation in MCM-41, part C. For MCM-41, the strongest bands relative to those of the silica host structure appear between 1000 and 1250 cm^{-1} and are due to Si−O asymmetric stretching vibrational modes; the band at ca. 785 cm^{-1} can be attributed to the Si−O symmetric vibrational mode, and the Si−O−Si bending vibration is found at ca. 475 cm^{-1}. The presence of water molecules is shown by the strong band at ca. 1623 cm^{-1}. The APTES-modified MCM-41 shows a band at ca. 3249 cm^{-1} characteristic of the NH_2 groups and a band at ca. 2931 cm^{-1} characteristic of asymmetric vibrations of the CH_2 group of the propyl chain of the silylating agent.[27] For $Eu_8P_4W_{43}$, the range of 1000−700 cm^{-1} contains three characteristic bands attributable to asymmetric stretching vibrations of the bridge (W−O_b-W) and of terminal bonds (W−O_t); additionally, in the range of 1100−1000 cm^{-1}, P−O asymmetric stretching vibrational bands appear.[28] We also note that the splitting of the characteristic P−O asymmetric stretching vibration found between 1100 and 1000 cm^{-1} suggests a decrease in the PO_4 group symmetry by coordination of the lanthanide ions to the ligand.[28]

By comparing the FTIR spectrum of MCM-41 samples (see Figure 8) before, part B, and after encapsulation of $Eu_8P_4W_{43}$, part C, we find that the spectrum displayed in part C shows characteristic absorption peaks of both $Eu_8P_4W_{43}$ and MCM-41. Some bands are hidden upon formation of the composite—e.g., the 896.1 and 765.3 cm^{-1} bands as well as bands around 1100 cm^{-1}—due to the dominating intensity of bands associated with MCM-41. As suggested by the spectra, generally, M−O_t stretching vibrations, which can be considered as pure vibration, show frequency increases as a result of anion−anion interactions. The M−O_t and P−O asymmetrical stretching frequencies of $Eu_8P_4W_{43}$ decrease from 955.1 to 939.5 cm^{-1} and 815.1 to 803.0 cm^{-1}, respectively, when the POM is inserted into MCM-41. This frequency decrease is attributed to the weakening of electrostatic anion−anion interactions, deriving from lengthening of the anion−anion distances in the silicate.[28]

Figure 9 shows Raman spectra of solid-state $Eu_8P_4W_{43}$ and the composite $Eu_8P_4W_{43}$/MCM-41. Similar Raman patterns for both samples are found. Both spectra have characteristic vibration peaks at ca. 218.2, 962.5, and 978.5 cm^{-1}, assigned to symmetric stretching γ_s (W−O_t, where O_t represents a

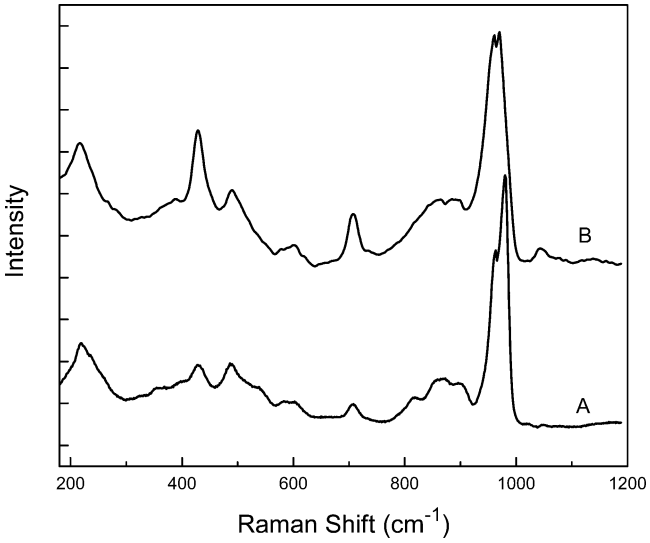

Figure 9. Raman spectra of (A) solid $Eu_8P_4W_{43}$ and (B) composite $Eu_8P_4W_{43}$/MCM-41; excitation wavelength of 615 nm.

terminal oxygen), asymmetric stretching γ_{as} (W−O_t), and symmetric stretching γ_s (W−O_i, where O_i represents the bridging oxygen between the internal phosphorus heteroatom and tungsten adducts), respectively; the relative weak bands at ca. 374, (860, 890, 912) and 1015 cm^{-1} are assigned to bending δ (W−O−W), γ_s (W−O−P), and γ_{as} (W−O−P), respectively. It is further to be noted that certain Raman bands for the composite vis-à-vis the respective bands for solid-state $Eu_8P_4W_{43}$ show blue shifts, e.g., 218.2 to 215.7 cm^{-1} for γ_s (W−O_t); 962.5 to 960.7 for γ_{as} (W−O_t); and 978.5 and 968.9 for γ_s (W−O_i).

On the basis of the assignments above, an obvious explanation for the band shifts and their direction is that host−guest interaction between the negatively charged terminal oxygen and the $-NH^{3+}$ terminal functional group on the wall of MCM-41, which although weak, can be expected to promote redistribution of local electrons on the polyoxometalate. The redistribution can be expected to decrease the electron densities of adjacent O, P, and W atoms, leading to an increase in bond lengths of W−O and P−O and an associated red shift as indicated by IR spectra. It is also important to notice that, for the Raman investigations, the vibration bands of polyoxometalate complexes shift toward higher energies providing evidence for an increase in polyoxometalate stability.[29]

IV. Conclusion

In summary, a polyoxometalate, $Eu_8P_4W_{43}$, was introduced into the mesoporous molecular sieve material MCM-41 under weakly acidic pH. On the basis of emission, excitation, FTIR, solid-state NMR, and Raman scattering measurements, the geometry of the polyoxometalate ions were deduced to be preserved inside the channel of MCM-41, although some weak microenvironmental perturbation exists. Furthermore, by way of comparison of FTIR and Raman band positions, we suggest that the incorporation of $Eu_8P_4W_{43}$ is facilitated by host−guest interaction between the negatively charged terminal oxygen and the $-NH^{3+}$ terminal functional group on the wall of MCM-41, at an appropriate pH. Due to its well-organized stable structure and luminescent property, such a composite might represent a new material with potential applications as a photoluminescent device or phosphor.

Acknowledgment. D.L.A. thanks the NSF and DoD-ARO for support of this work, in part, through the following awards: (1) NSF-IGERT Program under Grant DGE-9972892, (2) NSF-MRSEC Program under Grant DMR-0213574, and (3) DoD-ARO under Cooperative Agreement DAAD19-01-1-0759. L.C.F. thanks the NSF and NIH for support through Grants NSF-CHE 0414218 and NIH-S06 GM60654 (SCORE), respectively. T.P. thanks the following agencies for the following Grants: NSF for CAREER CHE-0237612, ACS Petroleum Research Fund (PRF Grant No. 39827-G5M), and NIH for subproject under P20-17716, COBRE.

References and Notes

(1) Coronado, E.; Gomez-Garcia, C. J. *Chem. Rev.* **1998**, *98*, 273.
(2) Briand, L. E.; Baronetti, G. T.; Thomas, H. J. *Appl. Catal., A* **2003**, *256*, 37.
(3) Mizuno, N.; Misono, M. *Chem. Rev.* **1998**, *98*, 199.
(4) Inouye, Y.; Tokutake, Y.; Yoshida, T.; Seto, Y.; Hujita, H.; Dan, K.; Yamamoto, A.; Nishiya, S.; Yamase, T.; Nakamura, S. *Antiviral Res.* **1993**, *20*, 317.
(5) Casan-Pastor, N.; Baker, L. C. W. *J. Am. Chem. Soc.* **1992**, *114*, 10384.
(6) Muller, A.; Peters, F.; Pope, M. T.; Gatteschi, D. *Chem. Rev.* **1998**, *98*, 239.
(7) Tomsa, A.-R.; Muresan, L.; Koutsodimou, A.; Falaras, P.; Rusu, M. *Polyhedron* **2003**, *22*, 2901.
(8) Xu, L.; Wang, E.; Li, L.; Kurth, D. G.; Du, X.; Zhang, H.; Qin, C. *New J. Chem.* **2002**, *26*, 782.
(9) Xu, L.; Zhang, H.; Wang, E.; Kurth, D. G.; Li, Z. *J. Mater. Chem.* **2002**, *12*, 654.
(10) Damyanova, S.; Dimitrov, L.; Mariscal, R.; Fierro, J. L. G.; Petrov, L.; Sobrados, I. *Appl. Catal., A* **2003**, *256*, 183.
(11) Zhao, Z.; Ahn, W.; Ryoo, R. *Stud. Surf. Sci. Catal.* **2003**, *146*, 657.
(12) Lindlar, B.; Lüchinger, M.; Röthlisberger, A.; Haouas, M.; Pirngruber, G.; Kogelbauerb, A.; Prins, R. *J. Mater. Chem.* **2002**, *12*, 528.
(13) Kozhevnikov, I. V.; Kloetstra, K. R.; Sinnema, A.; Zandbergen, H. W.; van Bekkum, H. *J. Mol. Catal. A: Chem.* **1996**, *114*, 287.
(14) Jalil, P. A.; Al-Daous, M. A.; Al-Arfaj, A. R. A.; Al-Amer, A. M.; Beltramini, J.; Barri, S. A. I. *Appl. Catal.* A **2001**, *207*, 159.
(15) Kurth, D. G.; Volkmer, D. *Polyoxometalate Chem.* **2001**, 301.
(16) Kaleta, W.; Nowińska, K. *Chem. Commun.* **2001**, 535.
(17) Xu, W.; Luo, Q.; Wang, H.; Francesconi, L. C.; Stark, R. E.; Akins, D. L. *J. Phys. Chem. B* **2003**, *107*, 497.
(18) Zhang, C.; Howell, R. C.; Scotland, K. B.; Perez, F. G.; Todaro, L.; Francesconi, L. C. *Inorg. Chem.* **2004**, *43*, 7691.
(19) Guo, H.; Zhang, X.; Aydin, M.; Xu, W.; Zhu, H.-R.; Akins, D. L. *J. Mol. Struct.* **2004**, *689*, 153.
(20) Liu, C. J.; Li, S. G.; Pang, W. Q.; Che, C. M. *Chem. Commun.* **1997**, 65.
(21) Zheng, S.; Gao, L.; Zhang, Q.; Zhang, W.; Guo, J. *J. Mater. Chem.* **2001**, *11*, 578.
(22) Nowińska, K.; Formaniak, R.; Kaleta, W.; Waclaw, A. *Appl. Catal., A* **2003**, *256*, 115.
(23) Naruke, H.; Yamase, T. *J. Lumin.* **1991**, *50*, 55.
(24) Zhang, H. Y.; Xu, L.; Wang, E. B.; Jiang, M.; Wu, A. G.; Li, Z. *Mater. Lett.* **2003**, *57*, 1417.
(25) Aquino, J. M. F. B.; Araujo, A. S.; Melo, D. M. A.; Silva, J. E. C.; Souza, M. J. B.; Silva, A. O. S. *J. Alloys Compd.* **2004**, *374*, 101.
(26) Wang, X.; Guo, Y.; Li, Y.; Wang, E.; Hu, C.; Hu, N. *Inorg. Chem.* **2003**, *42*, 4135.
(27) Joseph, T.; Deshpande, S. S.; Halligudi, S. B.; Vinu, A.; Ernst, S.; Hartmann, M. *J. Mol. Catal. A: Chem.* **2003**, *206*, 13.
(28) Jin, H.; Wu, Q.; Pang, W. *Mater. Lett.* **2004**, *58*, 3657.
(29) Tomsa, A. R.; Muresan, L.; Koutsodimou, A.; Falaras, P.; Rusu, M. *Polyhedron* **2003**, *22*, 2901.